A Self-sealing Fiber-reinforced Composite

Jericho L. Moll,[1] Scott R. White,[2,3] and Nancy R. Sottos[1,3,]*

[1]*Department of Materials Science and Engineering, University of Illinois at Urbana-Champaign, Urbana IL 61801, USA*

[2]*Department of Aerospace Engineering, University of Illinois at Urbana-Champaign, Urbana IL 61801, USA*

[3]*Beckman Institute for Advanced Science and Technology, University of Illinois at Urbana-Champaign, Urbana IL 61801, USA*

ABSTRACT: We describe a self-sealing plain weave E-glass epoxy composite with the healing components, microencapsulated dicyclopentadiene (DCPD), and paraffin wax coated Grubbs' catalyst dispersed throughout the matrix. In this work, sealing is assessed through use of a pressure cell apparatus to detect nitrogen flow through the thickness direction of a damaged composite. A controlled amount of microcracking is introduced through cyclic indentation of opposing surfaces of the sample. The resulting damage zone is proportional to the indentation load. We investigate the effect of DCPD microcapsule size and concentration on the self-sealing ability of plain weave E-glass epoxy composites. For $51\,\mu m$ diameter capsules ($6.5\,wt\%$), 67% of the self-sealing composite panels fully seal with no leaking, compared to 0% of the control panels with no sealing ability. When the amount of damage is reduced, 100% of the self-sealing samples resealed. Sealing performance decreases with smaller diameter capsules ($18\,\mu m$ diameter) and lower capsule concentrations ($2.7\,wt\%$), indicating that there is a minimum capsule size and concentration to deliver enough healing agent to seal a given damage volume.

KEY WORDS: self-healing, woven composite, microcrack.

INTRODUCTION

Fiber-reinforced composite tanks provide a promising method of storage for liquid oxygen and hydrogen for aerospace applications [1]. The inherent thermal fatigue of these vessels leads to the formation of microcracks, which allow gas phase leakage across the tank walls. Previously, much work was done to predict and quantify the leakage rate of gaseous fuel through damaged composite tank walls. Peddiraju et al. [2] numerically simulated the leakage rate of cryogens as a function of composite ply number, thickness, and damage opening in the material and compared these results with experimental findings.

Other experimental studies examined the effect of tensile fatigue damage on the leakage rate of hydrogen gas through a reinforced composite material at both room and cryogenic temperatures [3]. Additional studies by Bechel and Kim [4] and Bechel et al. [5] investigated how the density of thermally induced cracks varied with the number of cycles, ply thickness, and ply orientation. A later study, also by Bechel et al. [6], examined how permeability of helium gas through the composite changed with the number of thermal cycles and adjacent ply orientation.

Microencapsulated self-healing polymers, first demonstrated by White et al. [7], provide a method of repairing crack damage and recovering mechanical properties in polymeric materials. Self-healing was achieved in bulk thermosetting polymers [8–12], fiber reinforced composites [13–16], elastomers [17,18] coatings [19], and self-healing adhesives [20]. Work to develop smaller scale healing components capable of healing submicron crack separation was carried out by Blaiszik et al. [21].

Kessler et al. [13] and Kessler and White [14] incorporated dicyclopentadiene (DCPD) filled microcapsules and Grubbs' catalyst in graphite epoxy composites and achieved 38% recovery of interlaminar fracture toughness after healing at room temperature, and 66% recovery after healing at 80°C. More recently, Yin et al. [22,23] utilized an encapsulated epoxy resin and a latent imidazole curing agent in the matrix material of a woven glass/epoxy composite to promote healing (130°C for 1 h) of interlaminar fracture toughness. In an alternative approach, Pang and Bond [15,16], Williams et al. [24], and Trask et al. [25] embed hollow glass fiber reinforcement into glass and carbon fiber-reinforced composites. These hollow glass fibers are used to deliver either pre-mixed two part epoxy healing agent, or uncured epoxy resin and curing agent in separate fibers to the fractured section of the sample. When the composite is damaged the hollow fibers rupture causing the healing agent to flow into the damage and, after the application of heat, heal the crack.

Beiermann et al. [26] demonstrated the ability to heal puncture damage in polymeric membranes. Poly(dimethyl siloxane) (PDMS) self-healing functionality was introduced into the PDMS layer of a polyurethane/nylon/PDMS laminate using encapsulated PDMS resin and catalyst. As the embedded resin and catalyst capsules ruptured, the two components came into contact and healed the puncture damage, preventing gas from leaking through the laminate. Kalista et al. [27] studied a self-healing poly(ethylene-co-methacrylic acid) copolymer capable of thermally triggered molecular rearrangement, which allowed the material to regain its ability to hold pressure up to 3 MPa after projectile puncture damage. The self-healing functionality of this material is inherent in ionomers, which have a two-step healing mechanism involving elastic recovery followed by inter-chain diffusion self-healing.

In this article, we demonstrate the self-sealing ability of a woven glass fiber reinforced composite. Self-sealing functionality is introduced by the addition of an encapsulated healing agent, DCPD, and Grubbs' catalyst embedded in a polymer matrix composite. Sealing effectiveness is evaluated in samples with varying concentrations and sizes of microcapsules.

METHODS AND MATERIALS

Preparation of Sample Components

The healing agent, DCPD (Alpha Aesar) was distilled, stabilized with 150 ppm p-t-butyl-catechol and encapsulated in a urea–formaldehyde (UF) shell. Sealing performance was

Table 1. Summary of resin components for various sample types.

Sample type	Epoxy resin	E-glass reinforcement	Wax-protected catalyst	Wax micro-spheres	UF/DCPD micro-capsules
Self-sealing	X	X	X	–	X
Control 1	X	X	–	–	–
Control 2	X	X	–	X	X

investigated for two microcapsule sizes. The larger capsules, 51 μm in diameter, were manufactured by the oil in water emulsion *in situ* polymerization technique described by Brown et al. [28]. The smaller capsules, 18 μm in diameter, were manufactured in a similar fashion with a few procedural modifications. The amount of ethylene-maleic anhydride (EMA) was increased by 50% from the amount specified by Brown et al. [28]. The additional amount of stabilizing agent was needed because the surface area of the DCPD–water interface in the emulsion increases with decreasing droplet size. After completion of the encapsulation procedure, the excess EMA was eliminated by centrifuging the capsule solution in deionized water three times, decanting off the water after each cycle. The capsules were spray dried into a dry, free-flowing white powder.

As received first generation Grubbs' catalyst (Aldrich) was dissolved in benzene and freeze-dried as described by Jones et al. [29] and protected from deactivation by primary amines [11] in the epoxy matrix curing agent by paraffin wax using a procedure outlined by Rule et al. [30]. The 16 μm diameter Grubbs' catalyst and wax spheres were centrifuged three times in water to remove EMA, the emulsion stabilizing agent. The resulting solution was frozen in liquid nitrogen and freeze dried for approximately 48 h, resulting in a dry powder. Catalyst-free wax microspheres with an average diameter of 18 μm, were also produced by this protocol for control samples.

Sample Types

Self-sealing composite panels were fabricated along with two types of corresponding control panels. The components in each of these sample types are summarized in Table 1. Self-sealing samples consisted of epoxy resin, fiber reinforcement, microcapsules, and wax-protected catalyst microspheres. The first type of control specimens were made of epoxy resin and fiber reinforcement only and contained no self-sealing components (microcapsules or wax microspheres). The second type of control specimens were comprised of epoxy resin, fiber reinforcement, microcapsules, and wax microspheres without catalyst.

Sample Preparation

Composite panels were manufactured using a hand lay-up and compression molding technique similar to the method outlined by Kessler et al. [14]. The composite reinforcement consisted of four 150 mm × 200 mm plain weave E-glass (340 g/m^2) plies. We selected Epon 862 epoxy resin with Epikure 3274 curing agent mixed at a ratio of 100 : 40. The dry capsules and catalyst spheres were gently mixed into the resin followed by degassing under vacuum for at least 20 min. The lay-up was compacted under 170 kPa at 35°C for 72 h, creating samples with an average fiber volume fraction of 0.36 ± 0.03. Self-sealing and control (Type 2) samples were prepared with varying capsule concentrations.
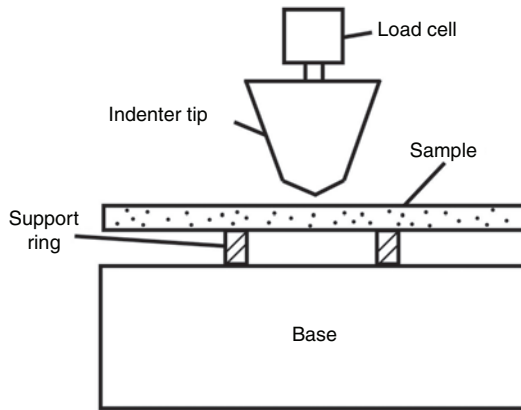
**Figure 1.** *Schematic of indentation apparatus to induce controlled damage in composite laminates.*
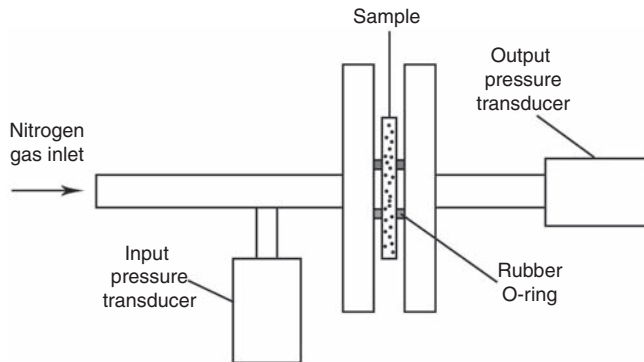
Figure 2. *Schematic of pressure cell set-up.*

Sample Testing

Each composite panel was sectioned into twelve 45 mm × 45 mm samples, which were all tested for healing. We developed an indentation protocol to induce consistent amounts of damage in the composite samples. A schematic of the indentation apparatus is shown in Figure 1. The square composite specimens were simply supported on a ring with an inner diameter of 24 mm and a height of 4 mm. The samples were damaged by driving a Vicker's diamond indenter tip into the sample with a predetermined velocity and load. The indenter tip was positioned above the middle of the sample and was cyclically driven into the surface of the specimen 10 times on each side. All samples, unless otherwise noted, were damaged with a maximum load of 410 N at a velocity of 150 µm/s. After the damage cycle, the samples were allowed to heal overnight at 30°C before testing continued.

Self-sealing functionality was evaluated using a pressure cell apparatus to quantify nitrogen flow through the damaged composites. The pressure cell (Figure 2) was designed for prior experiments by Beiermann et al. [26] to study healing of puncture damage in PDMS laminates. In the cell, the sample serves as a barrier between a pressurized chamber and the atmosphere. Pressure on both sides of the sample is monitored with time during the experiment.
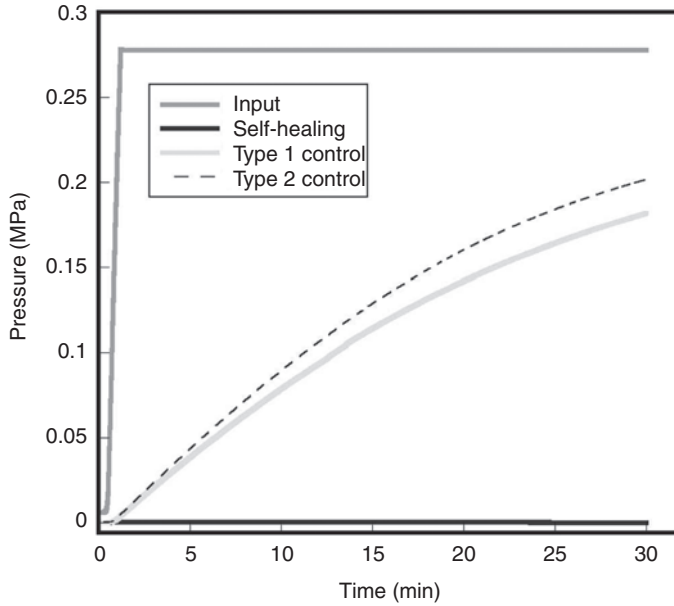
Figure 3. *Pressure evolution for representative sealed and control samples.*

Laminates were placed in the sample chamber and securely clamped between two O-rings to eliminate leakage from the cell. A computer-controlled regulator (EP211-X60-5 V, Omega) was used to ramp the applied pressure to the cell to 0.276 MPa. Pressure transducers were placed on either side of the sample. The first transducer measured the input pressure applied to the sample by the regulator. On the opposite side, the second transducer measured the output pressure due to nitrogen flow through the sample. If no output pressure was detected, then the specimen was fully sealed or there was insufficient damage to create an interpenetrating crack network that allowed nitrogen to flow through the specimen. Hence, sealing of damage was assessed by the change in pressure recorded by the second transducer. The input pressure and the time evolution of the output pressure measured for representative control Type 1 and Type 2 samples along with a fully sealed self-sealing sample are plotted in Figure 3.

Three different criteria were used to evaluate the self-sealing ability of composite specimens, the percentage of fully sealed samples, the initial slope, and the sealing efficiency (η_s). The percentage of samples which fully sealed was calculated based on the number of samples in which the output pressure did not increase by more than 0.07 kPa after 30 min of testing. In addition, for samples that do leak, we characterize the leakage rate by calculating the initial slope of the pressure evolution curve. A large slope corresponded to a high gas flow rate, while a small slope corresponded to a sample with low gas flow. A sealing efficiency was also calculated for all samples:

$$\eta_s = 1 - \frac{P(t)_{\text{out}}}{P(t)_{\text{in}}}\bigg|_{t\,=\,30\;\text{min}} \tag{1}$$

where pressure readings are taken after 30 min to allow sufficient time for the pressure evolution with time to develop, but sufficiently short to be used in laboratory experiments.
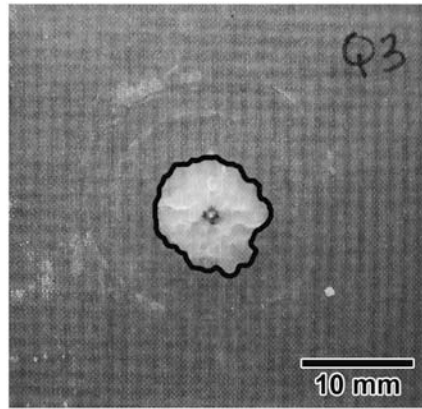
**Figure 4.** *Digital image of a Type 2 control sample with manual tracing around the damaged region.*

A sealing efficiency of zero corresponds to a final output pressure at 30 min equal to the input pressure (no sealing), while a fully sealed sample yields an efficiency of unity.

Damage Area Calculation

In both types of composite control samples, the opaque damage area was easily identified. As shown in Figure 4, the damaged region was manually traced using photo editing software. The damage area was then averaged over all samples of a given type. In self-sealing samples it was not possible to accurately identify the damage area using this method due to the dark purple color of the Grubbs' catalyst embedded in the specimens.

HEALING RESULTS

The effects of capsule size and concentration on sealing results were investigated for 51 and 18 μm diameter capsules at initial concentrations of 12.2, 6.5, and 2.7 wt% in resin. The capsules were sequestered in the resin-rich regions of the composite, causing local variations in concentration, which contributed to variations in sealing results. The concentrations of wax protected catalyst in the samples examined were 2.4, 2.6, and 2.7 wt%. The total amount of wax protected catalyst was kept constant, but the overall concentration changed due to differences in the mass of microcapsules added. Figure 5 compares the sealing performance of self-sealing specimens with varying microcapsule concentrations and diameters to that of the Type 1 control samples (no microcapsules or catalyst). All 12 specimens of each sample type in this data set (Table 2) were damaged at a maximum load of 410 N. Although 13% of the Type 1 control samples sealed, the 12.2 wt% and the 6.5 wt%, 51 μm diameter capsule self-sealing samples performed better than these control samples in all three of the sealing evaluation categories. Thirteen percent of Type 1 control samples appeared to seal because the damage in these samples did not percolate through the thickness of the laminate. The 6.5 wt% specimens with 51 μm diameter capsules had the highest percentage sealed and the highest sealing efficiency. In contrast, none of the 6.5 wt% specimens with 18 μm diameter capsules fully sealed, although their average leakage rate was smaller and average sealing efficiency higher than Type 1 control samples.
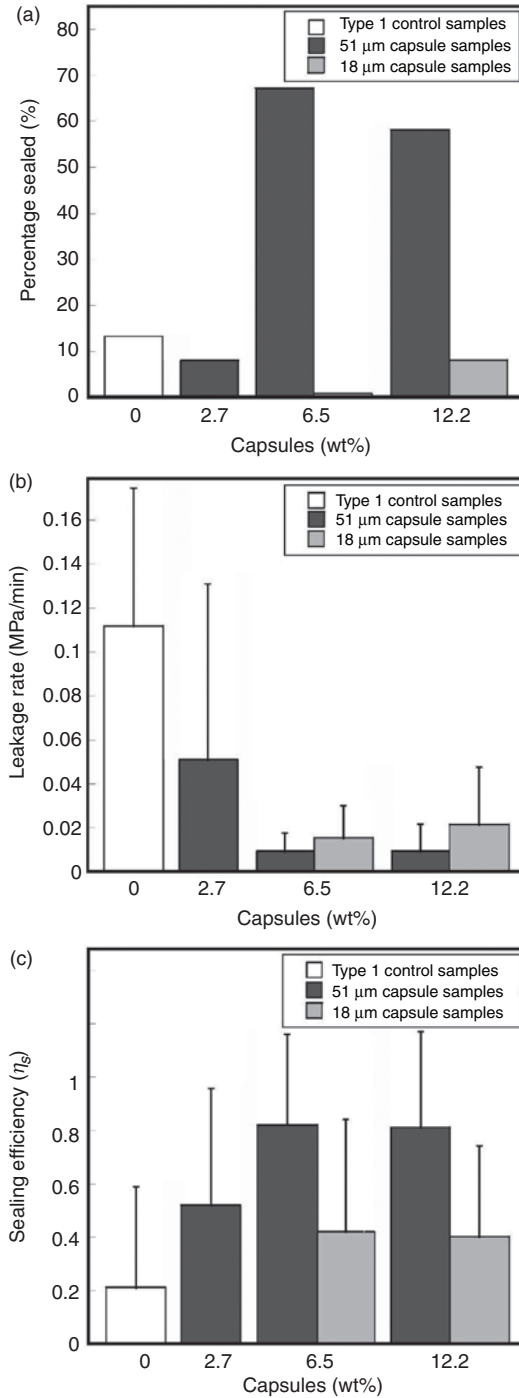
Figure 5. *Comparison of Type 1 control samples with self-sealing samples containing varying capsule sizes and concentrations: (a) percentage of samples sealing completely, (b) initial leakage rate in nonsealed samples, and (c) sealing efficiency. All samples were damaged with a peak force of 410 N. Error bars represent one positive standard devition.*

Table 2. Sealing summary for self-healing and control specimens.

Sample type	Capsule diameter (µm)	Capsule concentration (wt% in resin)	Peak load (N)	Samples sealed (%)	Leakage rate (MPa/min)	Sealing efficiency, η_s
Self-sealing	51	12.2	410	58	0.0091	0.81
Self-sealing	51	6.5	410	67	0.0092	0.82
Self-sealing	51	2.7	410	8	0.0509	0.52
Control-2	51	12.2	410	8	0.0176	0.43
Control-2	51	6.5	410	0	0.0831	0.14
Control-2	51	2.7	410	17	0.0876	0.31
Self-sealing	18	12.2	410	8	0.0214	0.40
Self-sealing	18	6.5	410	0	0.0151	0.42
Control-1	N/A	0	410	13	0.1117	0.21
Self-sealing	51	6.5	380	100	N/A	1.00
Control-2	51	6.5	380	25	0.0122	0.77

Specimens with 2.7 wt% 51 µm diameter capsules and both concentrations of 18 µm diameter capsules have a low sealing percentage, but a lower average leakage rate and higher average sealing efficiency than Type 1 controls. The sealing data for these specimens suggests that insufficient amounts of healing agent are delivered to the damaged region for full sealing of crack networks.

The sealing performance of Type 2 control specimens was also investigated and compared to corresponding self-sealing specimens with various capsule concentrations for the 51 µm diameter specimens. For all three capsule concentrations investigated, the self-sealing samples performed better than the respective Type 2 control samples.

The effect of peak damage load on the sealing results was also investigated by damaging 6.5 wt% 51 µm capsule Type 2 control and self-sealing samples at a lower peak load of 380 N (instead of the standard 410 N used for all other samples). A summary of the sealing results for these samples is provided within Table 2. All of the self-sealing samples sealed fully in these tests (100%), compared to 25% for the control samples. This result indicates that there is a maximum peak load below which 100% sealing can be achieved for a given capsule size and concentration.

Damage Characterization

To further understand the relationship between capsule size/concentration and sealing performance, we characterized the area of the damage zone in both types of control samples and compared the crack density in cross-sections of both self-sealed and Type 2 control specimens. The damage zone area of the control samples was analyzed from digital specimen images acquired after indentation (Figure 4). The damage area, plotted in Figure 6, increased with increasing capsule concentration and size. Although increasing the capsule concentration increases the amount of DCPD delivered to the crack, it also increases the amount of crack damage, suggesting that an optimum capsule concentration exists for a given amount of damage. For the self-sealing samples with 51 µm diameter capsules, the best sealing performance was achieved with 6.5 wt% capsule specimens. The higher capsule concentration (12.5 wt%) specimens led to a larger amount of damage, which could not be filled as effectively with capsules of this size. The lower capsule concentration (2.7 wt%) specimens had less damage, but insufficient amounts of healing agent for complete sealing.
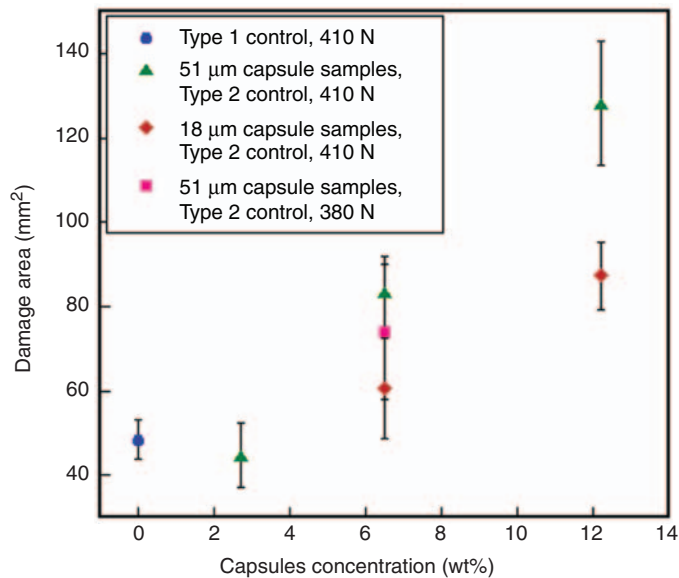
Figure 6. *Composite damage area as a function of damage load, capsule size, and capsule concentration. Error bars represent one standard deviation.*

Similarly, samples with 18 μm capsules had less damage area than the 51 μm capsule samples, but the percentage of samples that sealed was substantially lower. Thus, smaller capsules do not deliver a sufficient amount of DCPD to seal the damage.

The crack network was evaluated by comparing polished cross-sections of damaged regions in the composite specimens. Tiled scanning electron microscope images are shown in Figures 7 and 8 for Type 2 control and self-sealing samples with 12.2 wt% 18 μm capsules and 6.5 wt% 51 μm capsules, respectively. The cracks have been manually highlighted in white within the image of the Type 2 control sample in (a) and the self-sealing sample in (c). Only the highlighted cracks are shown for the control sample in (b) and the self-sealing sample in (d). Although cracks are still present in the self-sealing sample, enough of the cracks have healed to disrupt the percolation of crack damage, thus successfully sealing the sample.

As revealed in Figures 7 and 8, cracks in the composite samples run predominately between tows through resin-rich regions in the composite. The microcapsules are only located in these areas, therefore cracks that form inside fiber tows cannot heal due to a lack of healing agent. The region directly under the indenter tip has the largest crack separation, which decreases in the radial direction. The self-sealing cross-sections (Figures 7(c) and (d) and 8(c) and (d)) reveal a noticeable reduction in the number of cracks and a smaller crack separation when compared to the Type 2 control samples (Figures 7(a) and (b) and 8(a) and (b)). Cracks with smaller separation are more easily sealed due to the smaller volume of DCPD needed to fully seal the damage.

As seen in Figures 7 and 8, the location of the resin-rich regions within the composite vary from sample to sample. This heterogeneous distribution of fiber tows is typical in a low fiber volume fraction wet lay-up composite, but can cause variability in the crack path morphology. The scatter in leakage rates and sealing efficiencies observed for the samples in Figure 5 is likely due to this variability.
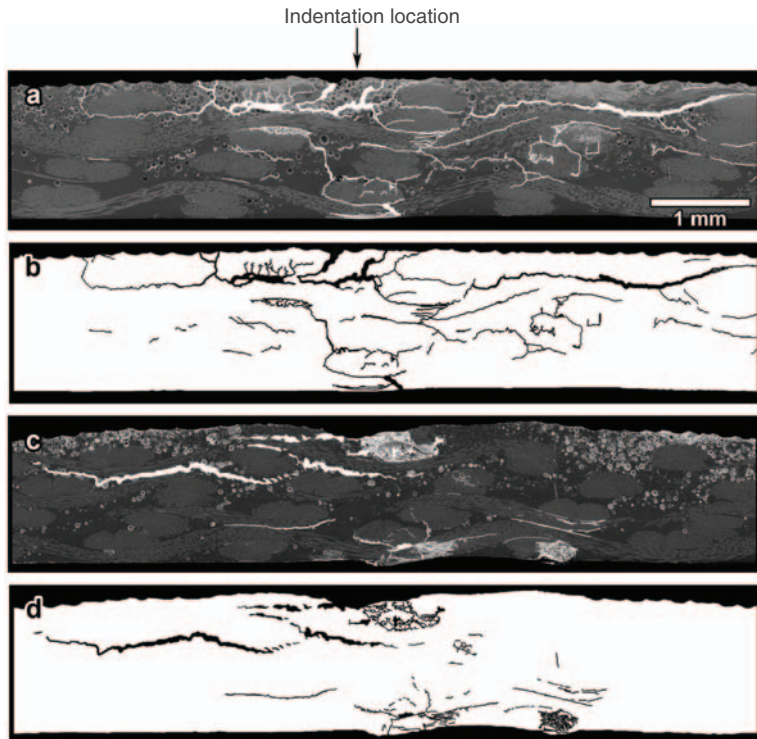
Indentation location
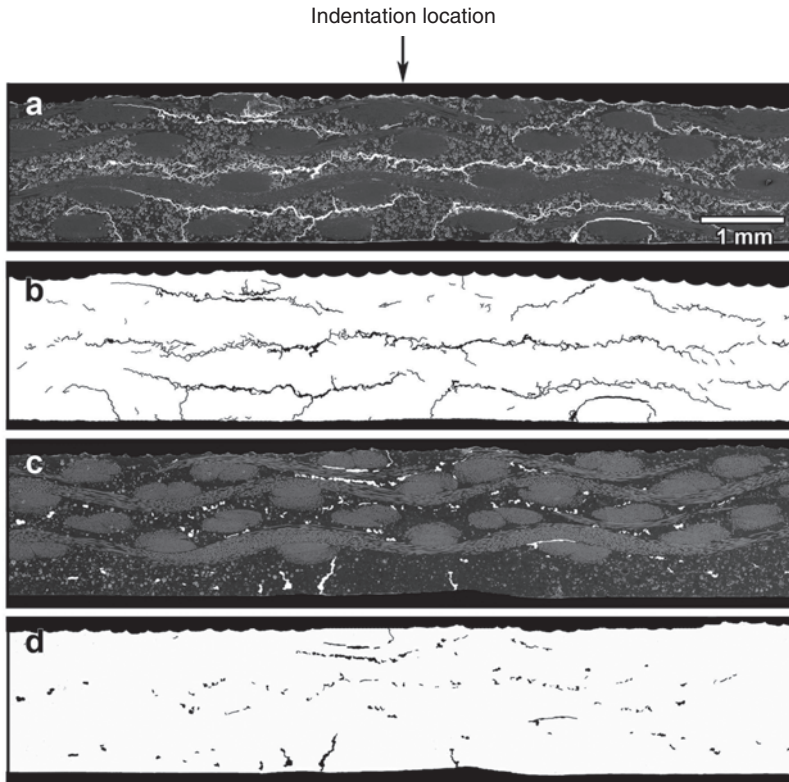
Figure 7. Comparison of crack damage in 12.2 wt%, 18 μm diameter capsule Type 2 control, and self-sealing specimens: (a) tiled SEM images of a polished cross-section of damaged area in a Type 2 control, (b) highlighted crack damage in black corresponding to the image in (a), (c) tiled SEM images of a polished cross-section of damaged area in a self-sealing specimen, (d) highlighted crack damage in black corresponding to the image in (c).

CONCLUSIONS

A self-sealing fiber-reinforced polymer matrix composite was achieved by incorporating UF-encapsulated dicyclopentadiene monomer and wax-protected Grubbs' catalyst into the matrix of a glass fiber-reinforced epoxy composite using a wet lay-up technique. The specimens were damaged by repeated indentation at prescribed loads. The connectivity of cracks in the damaged composite was evaluated by applying pressurized nitrogen gas to one side of the sample and monitoring the output pressure on the opposite side of the specimen.

Protocols were established to evaluate the self-sealing functionality of these composite specimens by monitoring the percentage of samples that fully sealed, initial leakage rate, and the sealing efficiency. The effects of capsule size and concentration on the self-sealing properties of the samples were evaluated. Specimens with 6.5 wt% 51 μm capsules performed the best in two of three sealing assessment categories.

Although the addition of microcapsules increases the fracture toughness of the matrix [8], increasing capsule concentration and size leads to an increase in damage area in

Figure 8. *Comparison of crack damage in 6.5 wt%, 51 μm diameter capsule Type 2 control, and self-sealing specimens: (a) tiled SEM images of a polished cross-section of damaged area in a Type 2 control, (b) highlighted crack damage in black corresponding to the image in (a), (c) tiled SEM images of a polished cross-section of damaged area in a self-sealing specimen, (d) highlighted crack damage in black corresponding to the image in (c).*

composites with both microcapsules and paraffin wax microspheres. The optimum capsule concentration for a given capsule size depends on the size of the damage volume compared to the volume of healing agent delivered.

Normal composite samples (Type 1 controls) were tested and compared to self-sealing samples. Specimens with 12.2 and 6.5 wt% 51 μm capsules outperformed the normal composites in all three sealing categories. All self-sealing samples, regardless of capsule size or concentration, show lower average leakage rate and higher average sealing efficiency compared to normal composites. Hence, optimized self-sealing composites show great potential to seal noncatastrophic crack damage in fiber-reinforced composite materials.

REFERENCES

1. Heydenreich, R. (1998). Cryotanks in Future Vehicles, *Cryogenics*, **38**: 125–130.

2. Peddiraju, P., Noh, J., Whitcomb, J. and Lagoudas, D.C. (2007). Prediction of Cryogen Leak Rate Through Damaged Composite Laminates, *Journal of Composite Materials*, **41**(1): 41–71.

3. Grenoble, R.W. and Gates, T.S. (2006). Hydrogen Gas Leak Rate Testing and Post-testing Assessment of Microcrack Damaged Composite Laminates, In: *47th AIAA/ASME/ASCE/ AHS/ASC Structures, Structural Dynamics, and Materials Conference*, Newport, Rhode Island, USA, 1–4 May.

4. Bechel, V.T. and Kim, R.Y. (2004). Damage Trends in Cryogenically Cycled Carbon/Polymer Composites, *Composites Science and Technology*, **64**: 1773–1784.

5. Bechel, V.T., Camping, J.D. and Kim, R.Y. (2005). Cryogenic/Elevated Temperature Cycling Induced Leakage Paths in PMCs, *Composites: Part B*, **36**: 171–182.

6. Bechel, V.T., Negilski, M. and James, J. (2006). Limiting the Permeability of Composites for Cryogenic Applications, *Composites Science and Technology*, **66**: 2284–2295.

7. White, S.R., Sottos, N.R., Geubelle, P.H., Moore, J.S., Kessler, M.R., Sriram, S.R., Brown, E.N. and Viswanathan, S. (2001). Autonomic Healing of Polymer Composites, *Nature*, **409**: 794–797.

8. Brown, E.N., Sottos, N.R. and White, S.R. (2002). Fracture Testing of a Self-healing Polymer Composite, *Experimental Mechanics*, **42**(4): 372–379.

9. Caruso, M.M, Delafuente, D.A., Ho, V., Sottos, N.R., Moore, J.S. and White, S.R. (2007). Solvent-promoted Self-healing Epoxy Materials, *Macromolecules*, **40**: 8830–8832.

10. Caruso, M.M, Blaiszik, B.J., White, S.R., Sottos, N.R. and Moore, J.S. (2008). Full Recovery of Fracture Toughness Using a Nontoxic Solvent-based Self-healing System, *Advanced Functional Materials*, **18**: 1898–1904.

11. Blaiszik, B., Caruso, M., McIlroy, D., Moore, J., White, S. and Sottos, N. (2009). Microcapsules Filled with Reactive Solutions for Self-healing Materials, *Polymer*, **50**: 990–997.

12. Wilson, G.O., Moore, J.S., White, S.R., Sottos, N.R. and Andersson, H.M. (2008). Autonomic Healing of Epoxy Vinyl Esters Via Ring Opening Metathesis Polymerization, *Advanced Functional Materials*, **18**: 44–52.

13. Kessler, M.R., Sottos, N.R. and White, S.R. (2003). Self-healing Structural Composite Materials, *Composites: Part A*, **34**: 743–753.

14. Kessler, M.R. and White, S.R. (2001). Self-activated Healing of Delamination Damage in Woven Composites, *Composites: Part A*, **32**: 683–699.

15. Pang, J.W.C. and Bond, I.P. (2005). A Hollow Fiber Reinforced Polymer Composite Encompassing Self-healing and Enhanced Damage Visibility, *Composites Science and Technology*, **65**: 1791–1799.

16. Pang, J.W.C. and Bond, I.P. (2005). 'Bleeding Composites' – Damage Detection and Self-repair Using a Biomimetic Approach, *Composites: Part A*, **36**: 183–188.

17. Keller, M.W., White, S.R. and Sottos, N.R. (2008). Torsion Fatigue Response of Self-healing Poly(Dimethylsiloxane) Elastomers, *Polymer*, **49**: 3136–3145.

18. Keller, M.W., White, S.R. and Sottos, N.R. (2007). A Self-healing Poly(Dimethylsiloxane) Elastomer, *Advanced Functional Materials*, **17**: 2399–2404.

19. Cho, S.H., Andersson, H.M., White, S.R., Sottos, N.R. and Braun, P.V. (2006). Polydimethylsiloxane-based Self-healing Materials, *Advanced Functional Materials*, **18**: 997–1000.

20. Miller, G.M. (2007). Self-healing Adhesive Film for Composite Laminate Repairs on Metallic Structures, Master of Science Thesis, Department of Aerospace Engineering, University of Illinois at Urbana-Champaign.

21. Blaiszik, B.J., Sottos, N.R. and White, S.R. (2008). Nanocapsules for Self-healing materials, *Composites Science and Technology*, **68**: 978–986.

22. Yin, T., Zhou, L., Rong, M.Z. and Zhang, M.Q. (2008). Self-healing Woven Glass Fabric/ Epoxy Composites with the Healant Consisting of Micro-encapsulated Epoxy and Latent Curing Agent, *Smart Materials and Structures*, **17**: 015019.

23. Yin, T., Rong, M.Z., Zhang, M.Q. and Yang, G.C. (2007). Self-healing Epoxy Composites −
    Preparation and Effect of the Healant Consisting of Microencapsulated Epoxy and Latent
    Curing Agent, *Composites Science and Technology*, **67**: 201−212.
24. Williams, G., Trask, R. and Bond, I. (2007). A Self-healing Carbon Fiber Reinforced Polymer
    for Aerospace Applications, *Composites: Part A*, **38**: 1525−1532.
25. Trask, R.S., Williams, G.J. and Bond, I.P. (2007). Bioinspired Self-healing of Advanced
    Composite Structures Using Hollow Glass Fibers, *Journal of the Royal Society Interface*, **4**:
    363−371.
26. Beiermann, B.A., Keller, M.W. and Sottos, N.R. (2009). Self-healing Flexible Laminates for
    Resealing of Puncture Damage, *Smart Materials and Structures*, **18**: 085001.
27. Kalista Jr, S.J., Ward, T.C. and Oyetunji, Z. (2007). Self-healing of
    Poly(Ethylene-Co-Methacrylic Acid) Copolymers Following Projectile Puncture, *Mechanics of
    Advanced Materials Structures*, **14**: 391−397.
28. Brown, E.N., Kessler, M.R., Sottos, N.R. and White, S.R. (2003). In Situ Poly(Urea-Formaldehyde)
    Microencapsulation of Dicyclopentadiene, *Journal of Microencapsulation*, **20**(6): 719−730.
29. Jones, A.S., Rule, J.D., Moore, J.S., White, S.R. and Sottos, N.R. (2006). Catalyst Morphology
    and Dissolution Kinetics of Self-healing Polymers, *Chemistry of Materials*, **18**: 1312−1317.
30. Rule, J.D., Brown, E.N., Sottos, N.R., White, S.R. and Moore, J.S. (2005). Wax-protected
    Catalyst Microspheres for Efficient Self-healing Materials, *Advanced Materials*, **17**(2): 205−208.